

## SECONDARY ELECTRON EMISSION YIELDS\*

I. Krainsky, W. Lundin, W. L. Gordon, and R. W. Hoffman  
Case Western Reserve University

### SUMMARY

The secondary electron emission characteristics for a variety of spacecraft materials have been determined under UHV conditions using a commercial double pass CMA which permits sequential Auger electron spectroscopic analysis of the surface. We have examined the transparent conductive coating indium tin oxide (ITO) on Kapton and borosilicate glass and indium oxide (IO) on FEP Teflon. Total yields vary slightly with samples and with substrates. The total SEE coefficient,  $\sigma_{\max}$ , ranges from 2.5 to 2.6 on as-received surfaces and from 1.5 to 1.6 on  $\text{Ar}^+$  sputtered surfaces with  $< 5$  nm removed.

For these measurements a cylindrical sample carousel provides normal incidence of the primary beam as well as a multiple Faraday cup measurement of the  $\sim$  nA beam currents. Total and true secondary yields are obtained from target current measurements with biasing of the carousel. A primary beam pulsed mode to reduce electron beam dosage and minimize charging of insulating coatings has been applied to  $\text{MgF}_2$  coated solar cell covers.

Electron beam effects on ITO were found quite important at the current densities necessary to do Auger studies ( $0.6 \mu\text{A}$  minimum or  $\sim 1 \times 10^{-4} \text{ A/cm}^2$ ) but relatively unimportant at the 10 nA levels used in short exposure methods or pulsed methods (150 nA peak, 2  $\mu\text{s}$ ) for obtaining SEE coefficients. Angle of incidence dependence for IO on FEP Teflon has been obtained for  $0.5 < EP < 5.0$  keV.

### INTRODUCTION

One result of the current interest in spacecraft charging phenomena has been the development in 1978 by NASA of a computer code - NASCAP - capable of providing a detailed picture of the charging process for realistic three-dimensional models of spacecraft (ref. 1). A major impediment to the use of NASCAP is the paucity of data for the secondary electron emission characteristics of actual spacecraft materials. Methods for obtaining these data from well-characterized surfaces using a commercial cylindrical mirror analyzer (CMA) were developed, tested on clean Ag and Cu surfaces, and applied to aluminum alloys with varying surface treatments typical of those used on spacecraft (ref. 2). Target current measurements gave electron yield data as a function of primary energy, EP. The CMA provided both the surface composition and the secondary electron energy distributions,  $N(E)$ , for a given EP from integration of the CMA output, operating in the standard derivative mode.

To overcome severe charging effects experienced with a thick insulating coating such as anodized samples we have developed a pulsed beam technique using sufficiently low dosage to permit measurements on thin insulating layers.

---

\*Work performed under NASA Grant No. NSG-3197

This method, together with that of short DC exposures to the primary beam, has been used to obtain secondary yields from thin ( $\sim 20$  nm) transparent conducting coatings, indium-tin oxide (ITO), on three insulating substrates: borosilicate glass, Kapton, FEP Teflon, and  $MgF_2$  on quartz. The influence of electron beam dosage effects has been explored in order to extrapolate the results back to typical current densities at the spacecraft surfaces. The effect of mild Ar ion sputtering of as-received surfaces has also been observed as a guide to changes in yield which may occur under prolonged plasma exposure in space. Secondary electron yields for  $0.5 \text{ keV} < EP < 5 \text{ keV}$  have been measured at varying angles of incidence.

## EXPERIMENTAL TECHNIQUES AND MODIFICATIONS

The electrons below 50 eV are usually termed "true secondaries" and the electrons above 50 eV termed "backscattered" (ref. 3). Thus, the true SEE coefficient  $\delta$  is just the number of true secondaries emitted per primary electron. Typically, measurements of conducting surfaces involve determination of the target current under two conditions:  $I_+$ , where backscattered electrons are rejected (biasing the target at +50 V relative to the grounded surroundings) and  $I_-$ , where all outgoing electrons are rejected (biasing the target at -50 V). The primary current,  $I_p$ , is found by displacing the carousel so that the beam enters the Faraday cup. As noted in reference 2,  $\delta = (I_+ - I_-)/I_p$  to a good approximation while the total SEE coefficient  $\sigma = 1 - I_-/I_p$  and includes elastically and inelastically backscattered electrons in addition to the true secondaries.

With thick insulating layers on the target surface, charging will take place, where the sign of the charge depends on whether  $\sigma$  is  $\lesssim 1$ . For our geometry, the CMA entrance grid subtends an angle of  $1.5 \pi$  steradians and is always grounded. Thus electric fields are developed as the target surface becomes charged.

### Pulsed Beam Techniques

To minimize charging effects on insulating layers as described above, we have introduced a pulsed beam technique together with a low energy electron flood gun to restore the surface to an uncharged state. If a single square current pulse of length  $\tau$  is incident on the insulator layer mounted on the target and the target is biased negatively to repel all secondaries then, referring to the equivalent circuit (figure 1(a)), the charge accumulated on the target is

$$q = \int_0^{\tau} I_- dt = \tau I_- \text{ and the potential drop across the input capacitor}$$

$C_1$  is  $V_- = q/C_1 = \tau I_-/C_1$ . Hence, as defined earlier, the total SEE coefficient  $\sigma = 1 - I_-/I_p = 1 - V_-/V_p$ . By observing  $V_-$  for a series of pulses at fixed EP, the presence of charging effects can be observed as a monotonic change in its value. Exposure of the surface of the insulating layer to low energy electrons from a flood gun will then restore the surface to a nearly uncharged state. Pulse measurements with +50 V applied to the target provide  $I_+$  so that  $\eta$  might be determined as well.

Beam pulses were produced through pulsing a beam blanking circuit. The process is illustrated schematically in figure 1(b). Single pulses from the pulse generator drive the blanking circuit which in turn controls the electron gun extractor potential. Target current pulses are typically 2  $\mu$ s duration with a 0.2  $\mu$ s rise time. They are registered by a sample-and-hold circuit for measurements by a DVM. The original pulses are stretched in time by a high input impedance follower, amplified by a factor of 100, and then enter the sample-and-hold circuit.

### Methods used for Secondary Yield Measurements

#### A - Short exposure to the primary beam

In measurements of secondary yield from conducting surfaces, DC exposure to the primary beam is a standard practice. To avoid over-exposure to the beam, particularly in the case of transparent conducting coatings, we have been careful to limit exposure time to a minimum, consistent with the observation of adequate signals. Thus we have used the beam blanking circuit in a manual operation mode to limit the time on the sample to 1 to 2 seconds. After completing beam alignment and focus of the primary beam,  $I_p$  is measured using the Faraday cup. The beam is then cut off and the carousel translated so that the beam will strike the sample at the new desired location. With the target biased at +50 V,  $I_+$  is found by disengaging the beam blanking circuit for  $\sim$  2 sec. The ammeter response time is  $\sim$  1 sec. The target is then biased to -50 V and  $I_-$  is found in another 2 to 3 sec. interval. Finally, the carousel is translated to bring the beam into the Faraday cup and again disengaging the blanking circuit to permit a second measurement of  $I_p$ . This procedure is repeated for each required value of EP.

From this series of measurements we obtain both  $\sigma$  and  $\delta$  as defined earlier. Also, by scanning across the Faraday cup we determine that the beam diameter is  $\sim$  2 mm. Typical primary currents ranged from 1 to 10 nA.

#### B - Pulsed beam measurements

A manually pulsed beam is employed, as described earlier, for the study of insulating surfaces and to avoid beam damage with conducting surfaces. The value of  $I_p$  is determined with the Faraday cup in place. During this time the beam is operated in a chopped mode to allow centering on the cup. A typical maximum value of the current pulses is  $\sim$  50 nA. After blanking, the carousel is shifted so that beam will strike the desired location on the sample. Then, with the target biased at -50 V relative to ground a 2  $\mu$ sec pulse is delivered and the value of  $I_-$  on the sample-and-hold circuit read from the DVM. Repetition of a single pulse in the region where  $\sigma > 1$  provides a quick test for charging, since  $\sigma_{obs}$  will drop monotonically if charging is present. In the presence of charging, use of the low energy flood gun between pulses assures that the sample surface is restored to its uncharged state, but does not guarantee the absence of charging during an individual pulse nor avoid field gradients in the sample near-surface region. Testing for charging in this latter case can be done by reducing pulse height and width and comparing the  $\sigma$

values obtained. At present, noise in the sample-and-hold circuit limits us to a pulse height of  $\sim 12$  nA in  $I_p$ .

Generally, only  $I_-$  was measured in this mode so the backscatter coefficient,  $\eta$ , was not obtained. Since  $\eta$  is not a large fraction of  $\sigma$  for insulators of low atomic number and is relatively constant in energy above a few hundred volts, an estimated value can be assigned without introducing serious Z-dependent uncertainties.

#### MATERIALS EXAMINED

Samples of three insulating materials, Kapton, FEP Teflon, and borosilicate glass coated with indium tin oxide (ITO) by the General Electric Company were provided to W. L. Lehn of the Air Force Materials Lab, Wright Patterson Air Force Base. Reactive sputtering techniques (ref. 4) were employed using a magnetron sputter gun, In/Sn targets and an oxygen + argon atmosphere. The compositions are nominally 90%  $\text{In}_2\text{O}_3$  and 10%  $\text{SnO}_2$  but the stoichiometries are uncertain. ITO film conductivity generally increases with the density of oxygen defects (ref. 5).

Table I gives a summary of the types of samples studied with nominal ITO thickness and back surface coating listed. We found that the ITO coating on the FEP sample had a very high-to-infinite resistance and showed sufficient charging that we could not make an Auger determination of In, Sn, or O present on the surface. An indium oxide (IO) coating, found by GE to be more compatible with FEP Teflon (ref. 6) was obtained. It had been prepared in essentially the same manner as the ITO coating. Samples are  $\sim 1$  cm x 1 cm, cut from 10 cm x 10 cm sheets of ITO on Kapton or IO on FEP Teflon and from 2.5 cm x 2.5 cm tiles of ITO on borosilicate glass with individual samples identified. All samples were inserted into the UHV system without prior surface cleaning except for blow-dusting with Freon gas.

The relative amount of In, Sn, and O in ITO, as well as other contaminants were obtained by AES methods. A surface contamination layer was present which increased the secondary yield compared to samples from which the contamination layer had been removed by Ar ion sputtering.

As a comparison with commercially available transparent conducting coatings (TCC) films, samples were obtained from Sheldahl. No nominal composition was supplied but our Auger analysis indicated the major components of TCC on Kapton were In, Sn, and O plus contamination.

$\text{MgF}_2$  coatings on quartz substrates were obtained from OCLI, and data obtained from both the coated and uncoated surfaces of the solar cell superstrates.

#### RESULTS AND DISCUSSION

The results will focus on yield data and include figures of  $\sigma(E)$  and/or  $\delta(E)$  for various coatings. Results of a study of the influence of the electron beam and sputtering of samples are included.

## Indium Tin Oxide Coatings

These data, in contrast with later pulsed results, have the advantage of containing both the total SEE coefficient,  $\sigma$  and true SEE coefficient  $\delta$  so are presented first, although they do represent a greater net exposure to the electron beam than do our pulse measurements. Furthermore, we note that earlier data obtained in this system for the SEE backscatter coefficient,  $\eta$ , of Ag ran (ref. 2) about 35% below the accepted value.<sup>†</sup> The reason for this discrepancy has not been determined but may be related to field distortions between the carousel and its surroundings during  $I_+$  measurements. Thus, we place greater emphasis on the  $\sigma$  values obtained here.

Typical results for as-received surfaces of ITO on Kapton and borosilicate glass and IO on FEP Teflon are presented in figures 2, 3, and 4. Primary beam currents and current densities are provided with each figure and SEE parameters tabulated. Particular samples cut from the sheet initially provided to us are identified for future reference. The current density values are only approximate since the beam profile is not rectangular. The data are remarkably similar considering the range of samples. Figure 5 presents the normalized  $\delta$  curves.

Differences between measurements on nominally similar specimens introduce the general question of reproducibility. Surface contaminants are the most important factor but surface roughness, general composition (particularly the variation in conductivity associated with varying O concentration), and electron beam effects cannot be neglected.  $\delta$  values obtained from three different locations on a single sample of IO on FEP and the variation for two different samples of ITO on borosilicate glass are small. We conclude that the uncertainties in a given measurement of  $\delta$  (and  $\sigma$ ) are approximately  $\pm 0.1$  with variations among samples occasionally outside this range.

The total SEE coefficient for the as-received surface of typical samples of Sheldahl TCC on Kapton and Teflon is not significantly different from the SEE coefficients from the GE as-received surfaces.

A comparison between pulsed beam and short exposure results for the GE samples was made using normalized curves to minimize the effect of variations among different samples of the same material and of possible effects of electron beam dosage as considered later. With the possible exception of IO on FEP Teflon no differences were encountered.

## Magnesium Fluoride Coated Solar Cell Covers

$MgF_2$  on fused silica required the pulsed beam technique because of the high (essentially infinite) sample resistance. In spite of the charging observed during SEE measurements, AES spectra were obtained without shifts of

---

<sup>†</sup> Bronshtein (ref. 7) using a  $4\pi$  collector geometry, quotes values of 0.38 at 1 kV and 0.41 at 4 kV while our values were 0.25 and 0.27 at these primary energies, with the  $1.5\pi$  solid angle geometry of our apparatus.

the Mg and F peaks, but AES spectra were not obtainable from the other side due to charging. Because of possible identification difficulties in coding of the coated side, both the MgF<sub>2</sub> and quartz surfaces of the OCLI standard solar cell covers were examined. Figures 6 and 7 present the  $\delta$  and  $\sigma$  data obtained for the MgF<sub>2</sub> and fused silica surfaces, respectively. All data were obtained by the pulsed beam method in which I<sub>+</sub> and I<sub>-</sub> were directly measured with  $\pm 50$  V potentials on the target. The data for the fused silica side are quite stable when compared to earlier samples, but the MgF<sub>2</sub> surface appears erratic. These data must be regarded as preliminary as we are not certain of the origin of the variations. As a result we have not listed the yield parameters.

#### Surface Contamination of ITO Coatings

The influence of surface contamination is best illustrated by comparison of SEE coefficients before and after argon ion sputtering. We examine these after presenting the AES evidence for a change in surface composition with sputtering. Auger spectra taken before sputtering of ITO on Kapton and IO on FEP Teflon show the presence of similar contaminants - C, S, Cl - on each of the as-received surfaces. After Ar<sup>+</sup> sputtering of  $\sim 1$  nm of the nominal 20 nm of ITO on Kapton film, there is little change in concentration except for the expected appearance of Ar and an increase in S. This particular increase correlated with results to be discussed later under electron beam damage. After  $\sim 4$  nm has been sputtered away (on a different sample) ITO on Kapton exhibits a significant clean-up of the surface contaminants. The In/Sn concentration increased but may be an artifact or a depth effect or be sample-dependent. This requires further study, as does our assumption that the 4 nm sputtering produces a "clean" ITO surface. It is, however, consistent with the results of electron beam damage studies discussed later.

Figure 8 shows the large changes in  $\delta$  values as a result of sputtering. The enhancement of the SEE coefficients due to contamination which exists prior to sputtering is evident and merits further study. Normalization of the  $\delta$  curves emphasizes a relative decrease in the high EP values for  $\delta$  with increased sputtering. This difference is unexpected, in the sense that the true SEE coefficients for most materials fit a common normalized yield curve.

#### Electron Beam Effects

Electron beam effects on surface composition have been well documented in the past, particularly in the case of Auger analysis where the measurement process can perturb the results. Such effects have a two-fold relevance to the present study. First, a knowledge of surface composition is essential to the general characterization of the surface for correlation with secondary emission yield. Second, the SEE coefficients (which are measured at a much lower current density than that used for Auger data) depend on electron beam effects. This, in turn, requires a detailed evaluation to predict their applicability to spacecraft charging.

In our preliminary studies of the SEE coefficients of ITO, we discovered that the values were dependent on whether the area under investigation had been previously exposed, as for example, in focussing the primary beam or in

previous Auger studies. After becoming aware of this problem we took data in the short exposure mode as outlined earlier and, when the pulsed beam circuit was available, we used this technique in the majority of cases to minimize dosages. This approach still does not provide a satisfactory answer to the question of the applicability of our results to spacecraft, in view of the extremely low current density in the plasma environment of the craft. To this end, we carried out an investigation of the electron beam dosage dependence of  $\sigma$  and of the Auger measurements of surface composition. This was accomplished by observing the time dependence of the parameter in question at a series of different primary current values, operating in the DC mode.

Measurements of  $\sigma(t)$  at a given current were done at an EP of 3 keV so that they are beyond  $EP_{max}$ . The primary electron gun was well stabilized before data were taken with the target biased at -50 V relative to ground. The beam size was determined in a position scan across the Faraday cup and typically had a diameter of  $\sim 0.8$  mm. A series of  $\sigma(t)$  values were obtained at each of 6 different values of  $I_p$  ranging from 10 nA to 36  $\mu$ A.  $I_p$  was checked before and after a given series of  $\sigma(t)$  measurements at that current to correct for a slight monotonic drift ( $\sim 2\%$ ) which continued to occur. Results are displayed in figure 9 with data points from 0.1 min to  $\sim 120$  min at each current. The earliest points are not indicated because of the difficulty of displaying the time scale appropriately but all values began at or near a  $\sigma$  of 1.25 to 1.3. Thus, while not shown, rapid drops in  $\sigma$  occurred, particularly at the higher currents. The 55 nA current curve started from a value close to that of the others but dropped abruptly to the "plateau" shown in figure 9. This effect has not been observed at other locations on the sample with other current levels nor has the reproducibility of the 55 nA result been checked. Wherever tested, we note that the effects illustrated here are not reversible with time.

For all  $I_p > 0.6 \mu$ A an obvious discoloration developed with a diameter about equal to the  $e^-$  beam spot area of  $5 \times 10^{-3} \text{ cm}^2$ . At the higher currents (36  $\mu$ A) perforation of the Teflon substrate resulted from the thermal damage. We speculate that contaminants, especially S, are brought to the surface and lead to a decreased secondary yield.

#### Angular Dependence of SEE Yield

It is well known that for metals as well as for semiconductors SEE coefficient  $\sigma$  increases with increasing incident angle  $\phi$  of the primary beam (ref. 7). In accordance with Bruining (ref. 8), primary electrons moving in straight paths penetrate to a smaller depth normal to the surface when the angle is slanting. Thus, secondary electrons are generated on the average at smaller depth and have an increased probability of escape. As a result  $\sigma$  is larger. Simple calculations based on this consideration give the following dependence of  $\sigma$  coefficient on the incident angle,  $\phi$ , relative to the specimen normal.

$$\ln \frac{\sigma(\phi)}{\sigma(0)} \approx x\alpha(1 - \cos \phi) \quad (1)$$

where  $x$  is the penetration length measured along the incident path, and  $\alpha$  is

the absorption coefficient. Of course, the constants  $\sigma_0$  and  $\alpha$  should depend upon the primary electron energy. Similar considerations apply to  $\eta$ .

Our aim was to investigate the angular dependence of  $\sigma$  and  $\eta$  coefficients for conducting coatings on Teflon and Kapton substrates. We constructed a new holder with a commutator for in-target current measurements using a Faraday cup with the sample at the focus of the CMA. The specimen rotates such that the incident electron beam varies from 0 to 90 degrees with respect to the specimen normal.

Figures 10 and 11 display experimental data ( $\sigma(\phi)$  and  $\eta(\phi)$ ) for IO on Teflon. Plotted in the form of equation (1), the normalized  $\sigma$  data are linear at EP = 5 keV but fall below the line at small values of  $\cos \phi$  and lower primary energies. The backscatter coefficient shows deviations for the higher energies.

### CONCLUSIONS

Our studies of the electron-induced secondary electron yields for various spacecraft materials may be summarized as follows.

1. Reliable pulsed beam methods have been developed for use with insulating samples.
2. Techniques using low incident electron currents ( $< 10$  na) must be used to avoid  $e^-$  beam damage to plastics coated with ITO. The decreased yields that follow are associated with surface compositional changes.
3. Significant surface contamination is present on as-received materials which results in increased SEE yields. The use of in-situ AES with SEE yield measurements is encouraged.
4. The incident angular dependence of  $\sigma$  and  $\eta$  of thin conducting coatings on plastics is consistent with a simple penetration depth model.

### REFERENCES

1. Katz, K., Cassidy, J. J., Mandell, M. J., Schuelle, G. W., Steen, P. G., and Roche, J. C.: The Capabilities of the NASA Charging Analyzer Program. Spacecraft Charging Technology - 1978, NASA Conf. Publ. 2071, 1979, p. 101.
2. Chase, R. W., Gordon, W. L., and Hoffman, R. W.: Appl. of Surf. Science 4, 271 (1980).
3. Whetten, N. Rey,: in Methods of Experimental Physics, edited by L. Marton (Academic Press, New York, 1967), Vol. 4A, Sec. 1.1.4, pp. 69-85.
4. Amore, L. J., and Eagles, A. E.: Materials and Techniques for Spacecraft Static Charge Control, Proceedings of the Spacecraft Charging Technology Conf. - 1976, Pike and Lowell, eds. NASA Tm X-73537, 1978, p.621.

5. Vossen, J.: RCA Review 32, 289 (1971).
6. Eagles, A. E., et al.: Spacecraft Static Charge Control Materials, AFML-TR-77-105 Part II (June 1977).
7. Bronshtein, I. M., and Fraimen, B. S.: Secondary Electron Emission, NAUKA (Science Publishers), Moscow (1969).
8. Bruining, H.: Physica 3, 1046 (1936).

TABLE I

Source	Front Surface Coating Nominal Thickness	Substrate	Back Surface Coating Nominal Thickness
GE (10248 K-2)	ITO <sup>a</sup> 20 nm	Kapton, 3 mil	Al 20 nm
GE (10248 T-1) <sup>b</sup>	ITO <sup>a</sup> 20 nm	FEP Teflon, 5 mil	Ag/Inconel 20 nm
GE	ITO <sup>a</sup> 20 nm	borosilicate glass (Corning 0211 Microsheet)	
GE <sup>c</sup> 4-18-9T1-34	IO 10 nm	FEP Teflon	
Sheldahl <sup>d</sup> G410620	TCC	Kapton 2 mil	Al
G409420	TCC	Teflon 2 mil (probably FEP Teflon)	Ag/Inconel
OCLI <sup>e</sup>	MgF <sub>2</sub>	Fused silica	

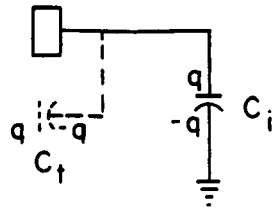
<sup>a</sup>Nominally 90% In<sub>2</sub>O<sub>3</sub> and 10% SnO<sub>2</sub> but uncertain stoichiometry. Prepared by reactive sputtering in an oxygen + argon atmosphere, using magnetron sputtering with in-situ RF activation.

<sup>b</sup>Film showed very high  $\rightarrow \infty$  resistance in two-probe measurement and exhibited serious charging effects in electron beam. ITO layer apparently deteriorated during storage.

<sup>c</sup>Obtained as replacement for original ITO on FEP Teflon film. Non-uniform in that showed large variations in resistance by two-probe measurement.

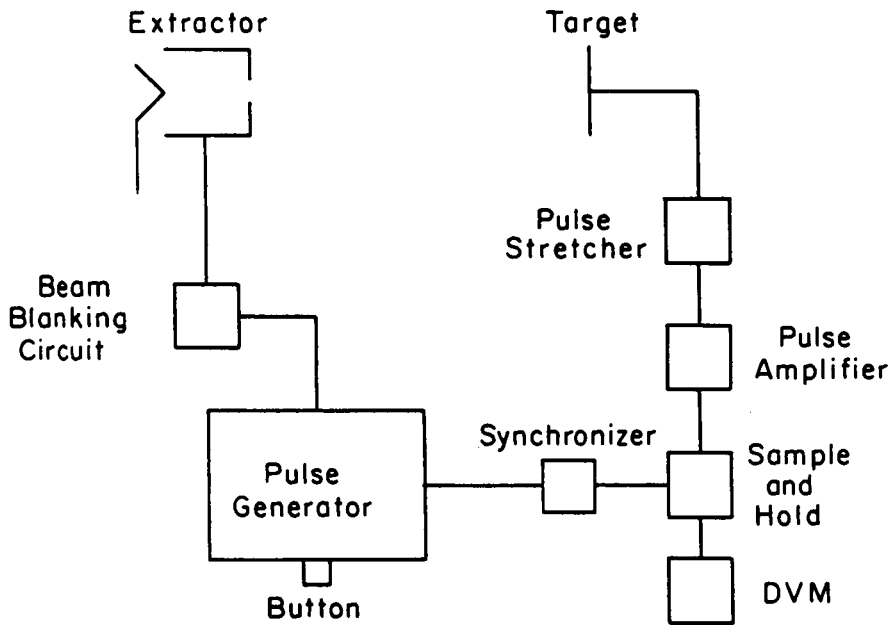
<sup>d</sup>Sheldahl, Northfield, Minnesota 55057. No information supplied on thickness of TCC nor composition. Resistivity given as  $\leq 250 \text{ K}\Omega/\square$ .

<sup>e</sup>Optical Coating Laboratory, Inc., Santa Rosa, California, 95403. No information was supplied.



( a )

Fig. 1(a). The equivalent circuit of the target showing the input capacitor,  $C_i$  and the sample capacitance between the sample surface and carousel,  $C_t$ .



( b )

Fig. 1(b). Block diagram illustrating the circuits used in the pulsed beam mode of operation.

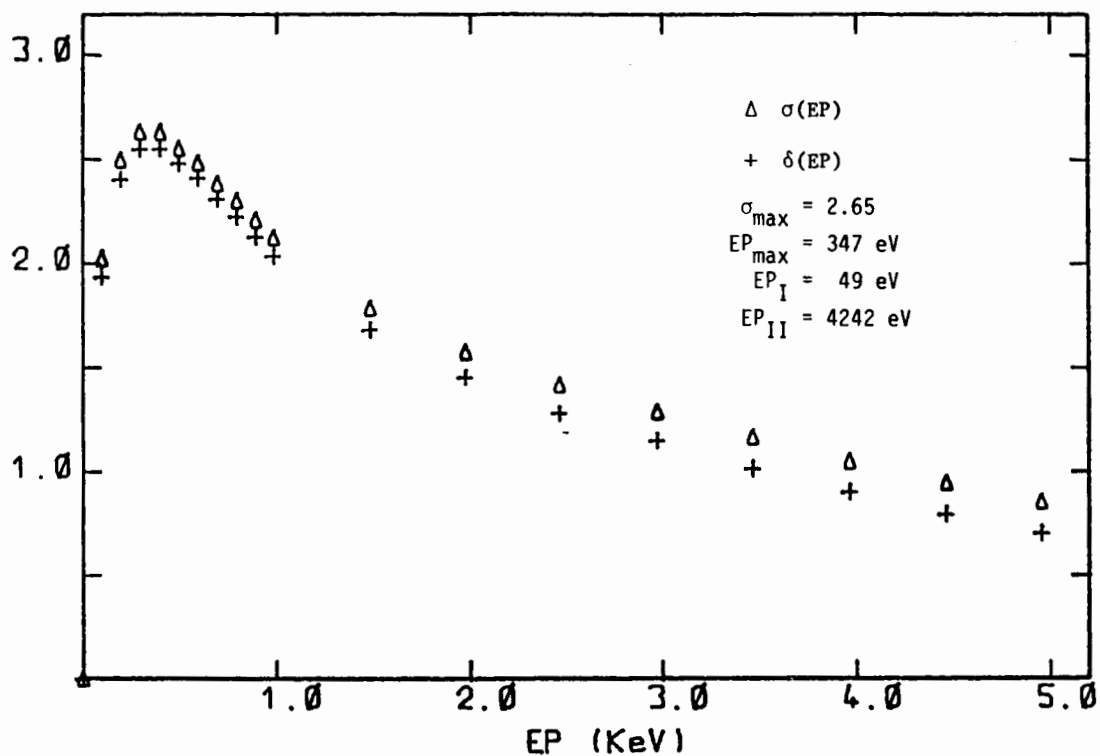


Fig. 2. SEE coefficients  $\delta$  and  $\sigma$  for ITO on Kapton, as-received surface. The short exposure method was used with  $J_p \sim 400 \text{ nA/cm}^2$  and  $I_p = 14 \text{ nA}$ . Sample K-85A.

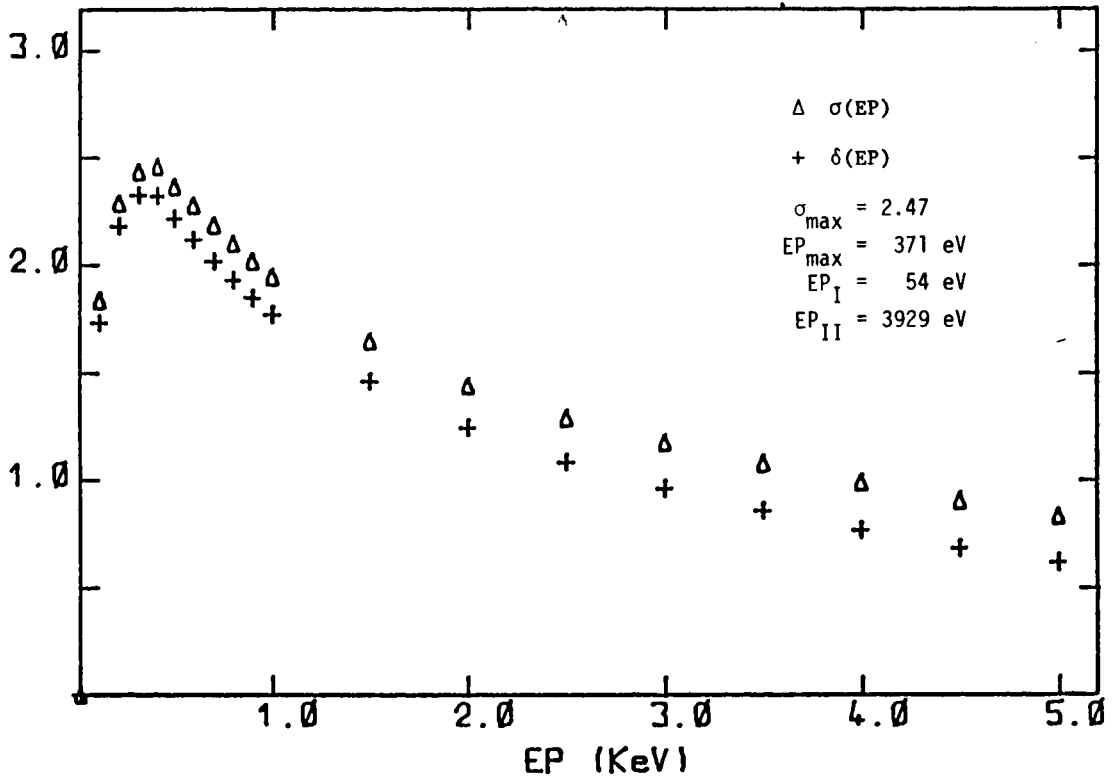


Fig. 3. SEE coefficients  $\delta$  and  $\sigma$  for ITO on borosilicate glass, as-received surface. The short exposure method was used with  $J_p \sim 300 \text{ nA/cm}^2$  and  $I_p = 10 \text{ nA}$ . Sample B-72.

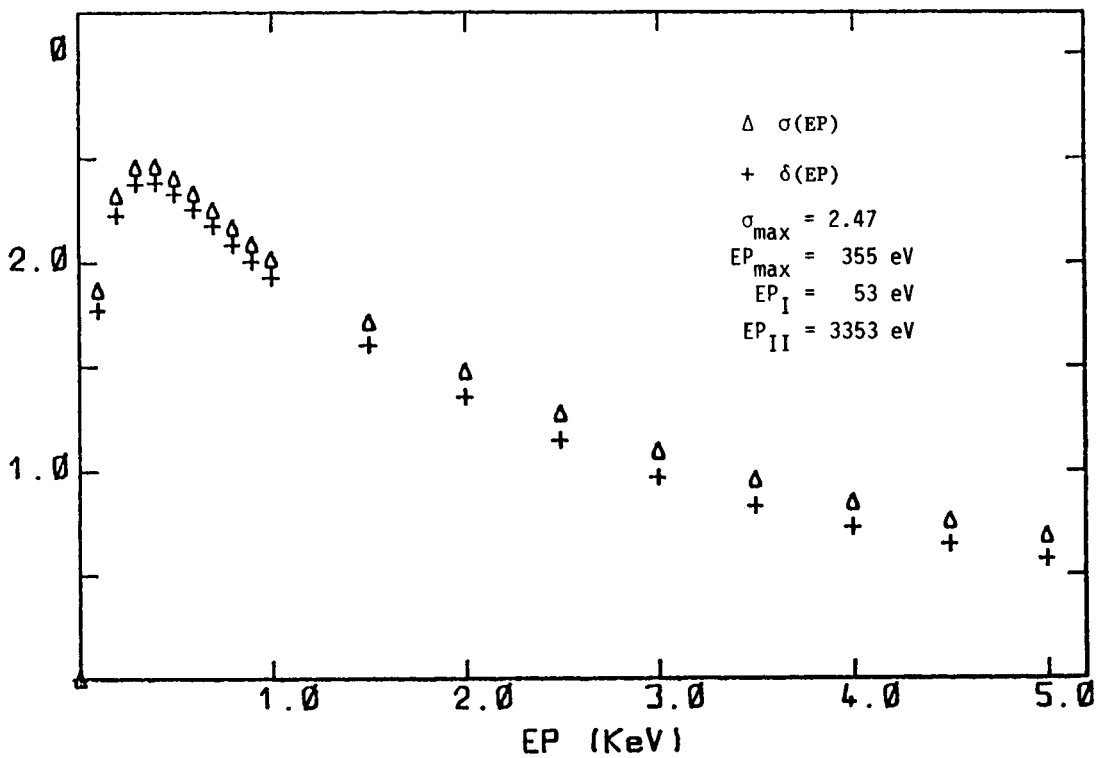


Fig. 4. SEE coefficients  $\delta$  and  $\sigma$  for IO on FEP Teflon, as-received surface. The short exposure method was used with  $J_p \sim 480 \text{ nA/cm}^2$  and  $I_p = 15 \text{ nA}$ . Sample T-86A.

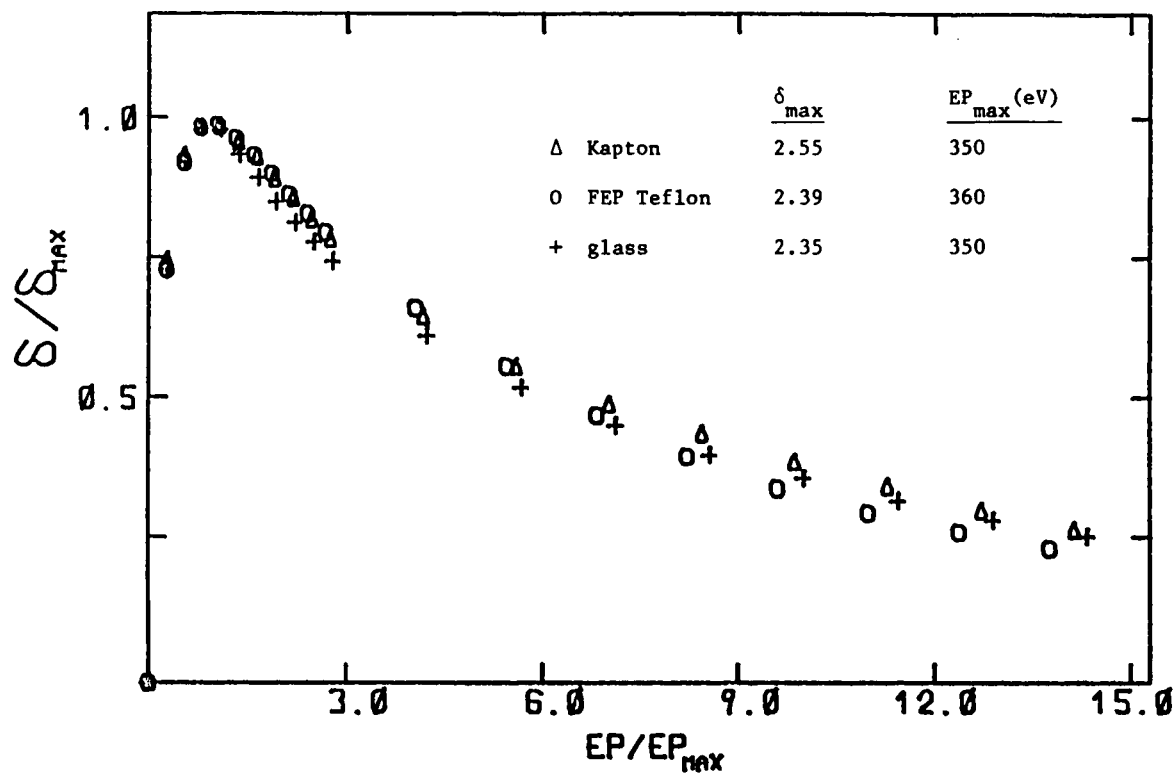


Fig. 5. Normalized  $\delta$  values for the as-received ITO films on Kapton and borosilicate glass and IO film on FEP Teflon. Samples and conditions identical to figures 2, 3, and 4.

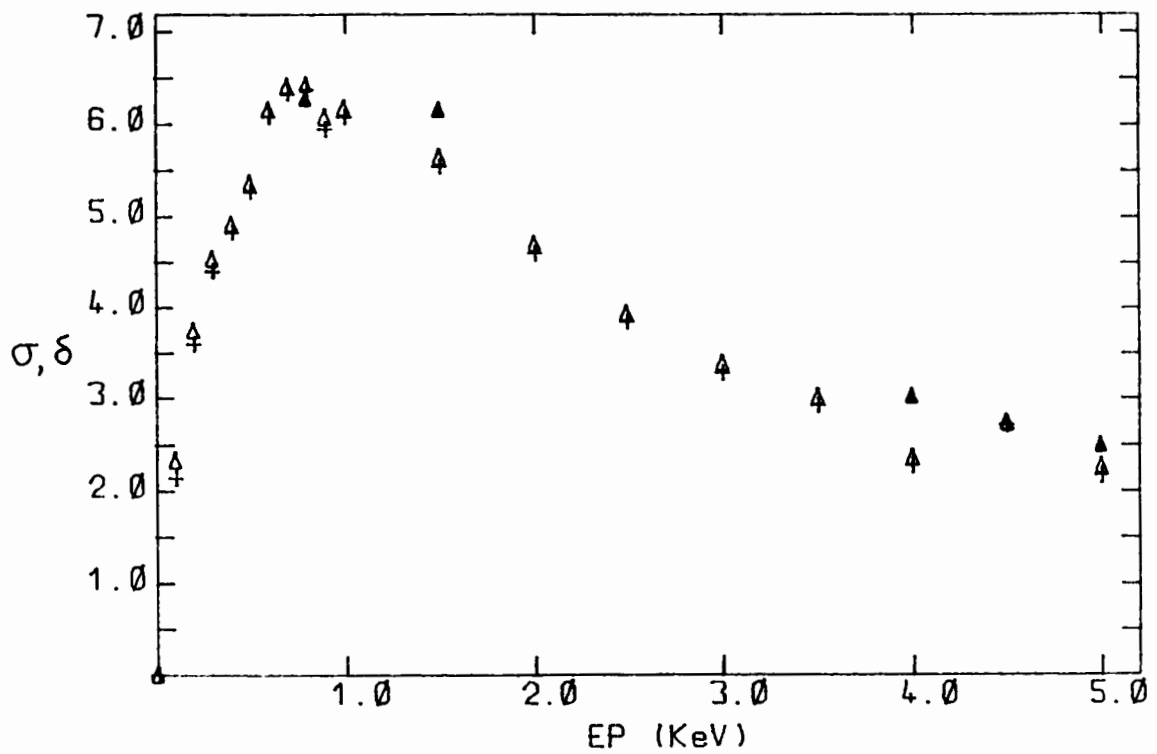


Fig. 6. Preliminary data for SEE coefficient  $\delta$  and  $\sigma$  for  $\text{MgF}_2$ , as-received surface. Single pulse method was used with  $I_p = 12$  nA in the pulse.

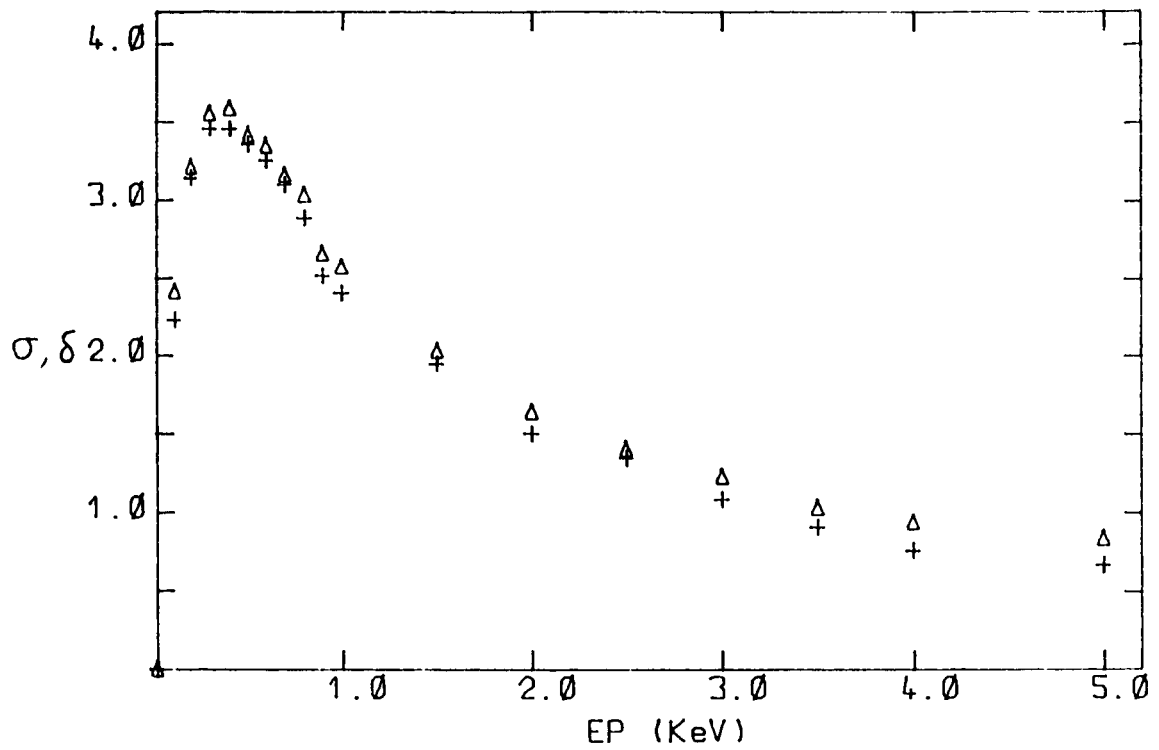


Fig. 7. Preliminary data for SEE coefficient  $\delta$  and  $\sigma$  for fused silica, as-received surface. Single pulse method was used with  $I_p = 12$  nA in the pulse.

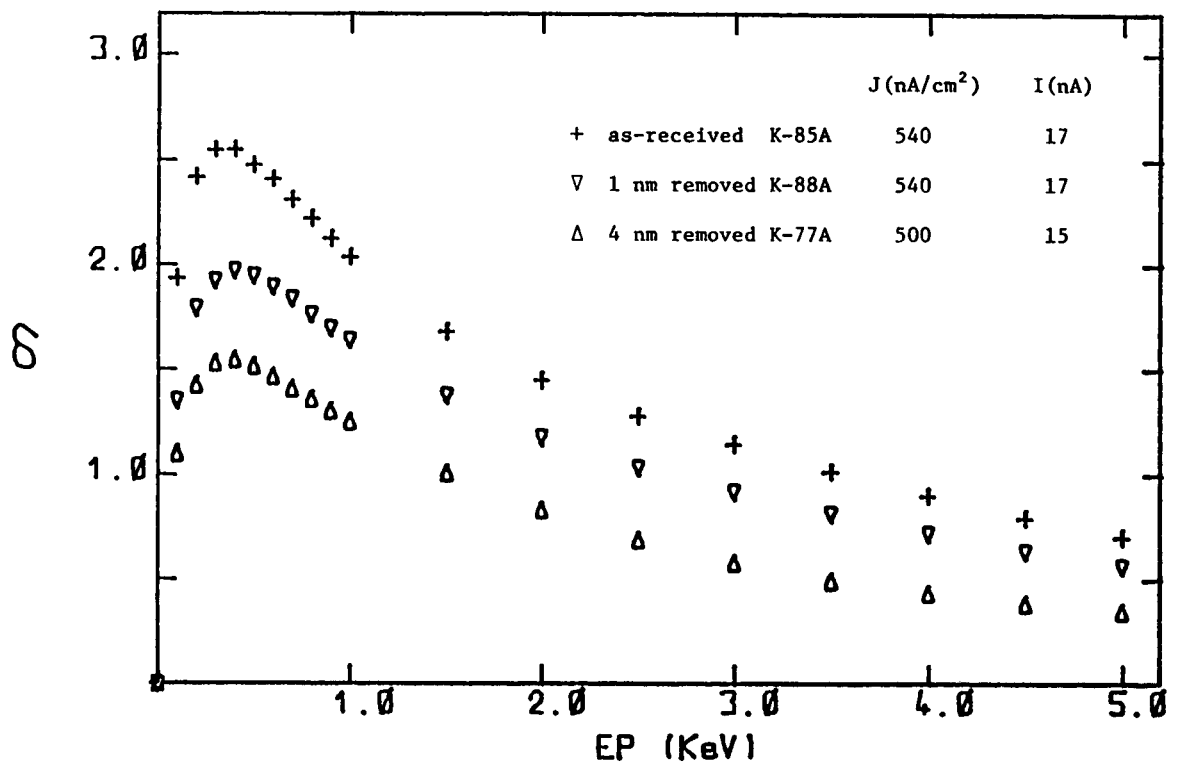


Fig. 8. Comparison of  $\delta(EP)$  for as-received and ion sputtered surfaces of ITO on Kapton. The short exposure method was used.

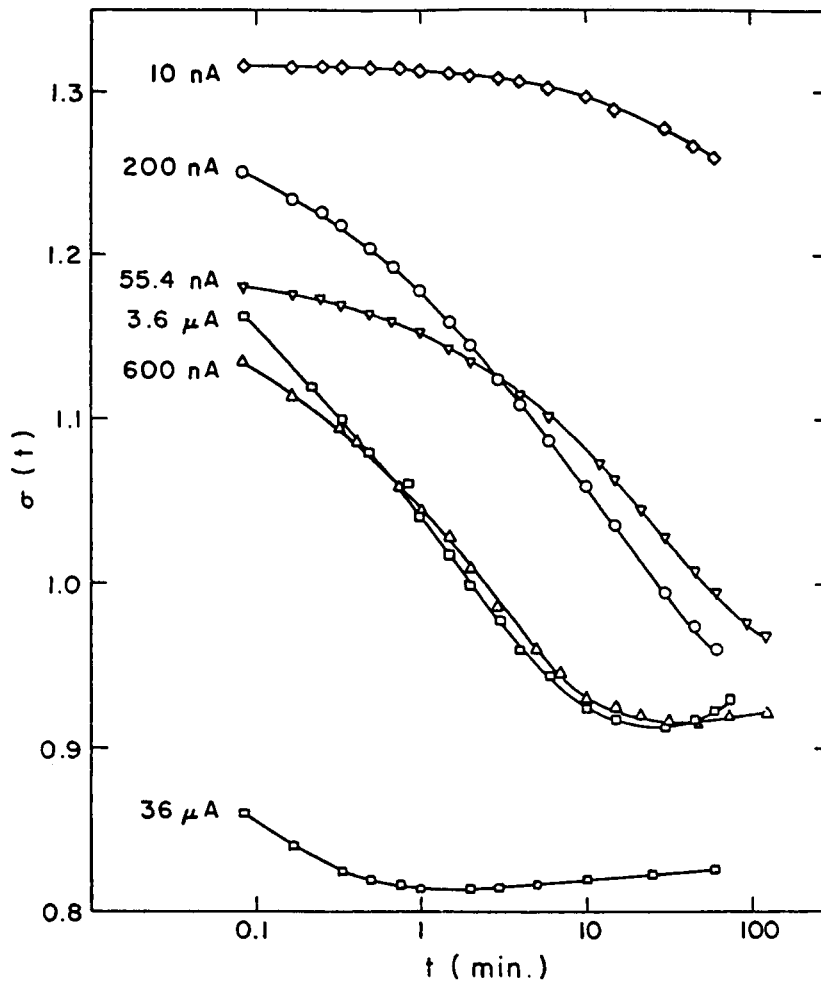


Fig. 9. Total SEE coefficient for ITO on Kapton as a function of time at  $EP = 3 \text{ keV}$  for different electron beam currents,  $I_p$ .

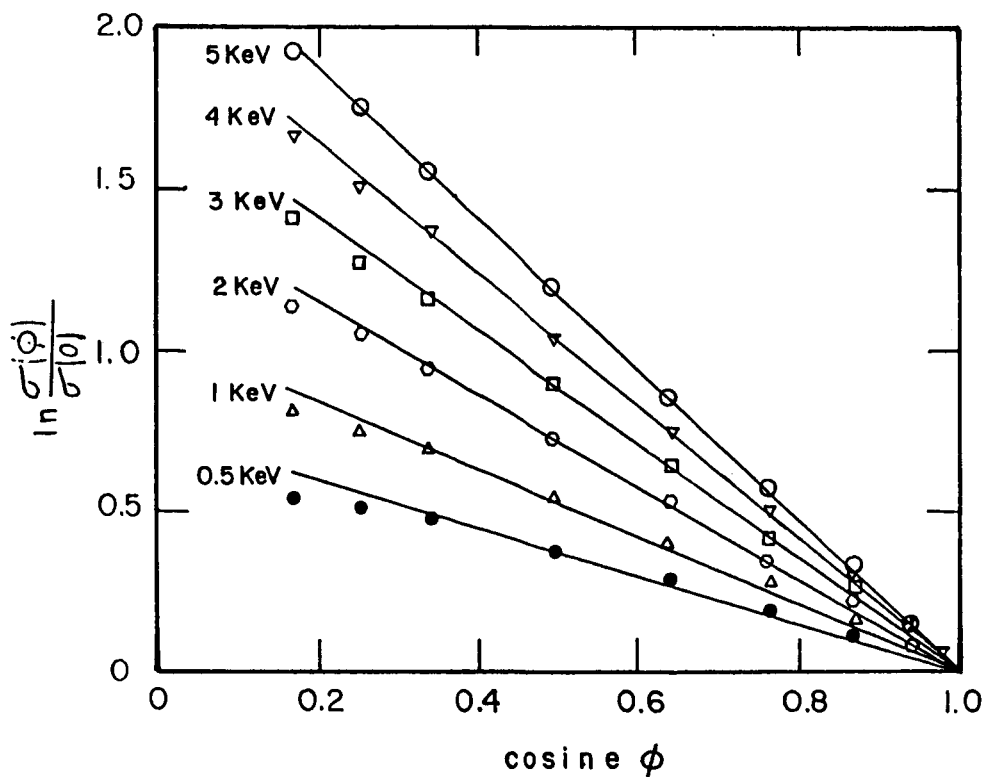


Fig. 10. Angular dependence of normalized SEE coefficient  $\sigma$  of IO on FEP Teflon for several primary beam energies.

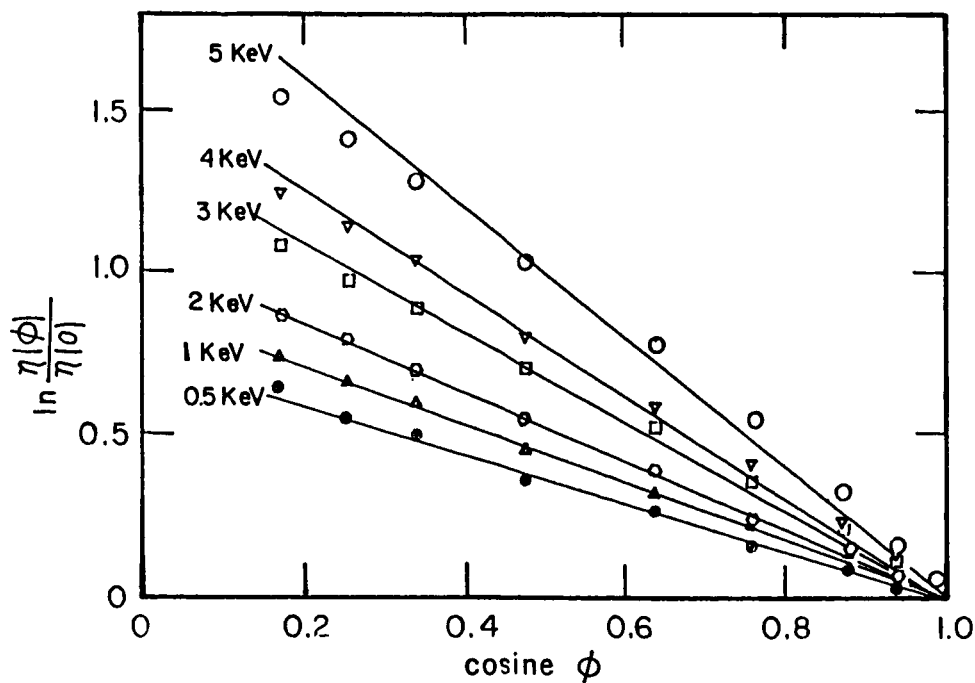


Fig. 11. Angular dependence of normalized SEE coefficient  $\eta$  of IO on FEP Teflon for several primary beam energies.